Received: 15 July 2020 | Accepted: 9 November 2020

DOI: 10.1002/pamm.202000308

In Silico Modeling of Coupled Physical-Biogeochemical (P-BGC) Processes in Antarctic Sea Ice

Andrea Thom[1,*] and **Tim Ricken**[1]

[1] Institute of Mechanics, Structural Analysis and Dynamics, Faculty of Aerospace Engineering and Geodesy, University of Stuttgart, 70569 Stuttgart, Germany

Antarctic sea ice formation in the Marginal Ice Zone (MIZ) and its mutual effects on ocean biology and chemistry is very sensitive to climate change. The formation of 'pancake' ice floes and the coupled physical-biogeochemical (P-BGC) processes can be modeled by using the continuum mechanical multi-phase description of the extended Theory of Porous Media (eTPM), and simulated with the Finite Element Method (FEM). The ice formation is described via a salinity-temperature equilibrium of the enclosed ocean water. The growth of the thriving ice algae, enclosed and attached to the pancake ice floes, is modeled with a phenomenological approach given with an ordinary differential equation.

1 Introduction

Phytoplankton (ice algae) growing in Antarctic sea ice constitutes an important factor for the food web as well as for the global carbon balance. The forming sea ice at the ocean-atmosphere interface in the Marginal Ice Zone (MIZ) of the Antarctic continent, the so-called 'pancake' ice floes, provide an optimal habitat for the growing phytoplankton, see Fig. 1 and Fig. 2. When sea ice forms from salty ocean water, the freezing ice crystals from freshwater molecules entrap ocean water in brine pockets. Ocean water contains e.g. nutrients, trace metals and the living sea ice algae, so that these are automatically entrapped in the forming pancake ice floes. Sea ice is characterized by steep gradients in temperature, salinity, light, and brine availability, which are, besides the availability of nutrients, major physical constraints to the growth of ice algae. Research is ongoing to include a sea ice biogeochemcial (BGC) component to large-scale physical (P) sea ice models to investigate mutual impacts on horizontal and vertical ice thickness distribution and BGC processes.

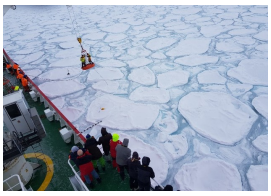

Fig. 1: Pancake formation in Antarctic MIZ seen from icebreaker *SA Agulhas II*

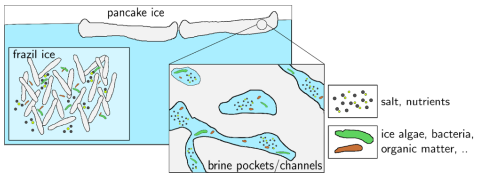

Fig. 2: Schematics of pancake ice floe and physico-biochemical inclusions

2 Constitutive Modeling

The underlying physical basis for ice formation is given via the continuum-mechanical framework of the *extended Theory of Porous Media (eTPM)*, see [1,2]. The biphasic model consists of an incompressible solid phase representing the pure ice $\varphi^{\mathbf{I}}$, frozen from freshwater, and the incompressible liquid phase representing the remaining and enclosed brine $\varphi^{\mathbf{L}}$. The brine is characterized by high salt concentrations, which is caused by the fact, that only the freshwater part of the ocean water freezes, and the salt molecules accumulate in the enclosed pockets, called brine channels. Hence, the liquid phase $\varphi^{\mathbf{L}}$ is a variable mixture of freshwater φ^{Lw} and salt φ^{Ls}. At thermal equilibrium, brine inclusions adjust their salinity S^{br} to the local freezing point given by the third-order fit according to [3] with $(1)_1$

$$S^{br} = -21.4\,\theta - 0.886\,\theta^2 - 0.0170\,\theta^3\,, \qquad \mathrm{n}^{\mathbf{L}} = -\mu\,\frac{S^{bulk}}{\theta}\,, \tag{1}$$

which suits well for BGC-models, cf. [4]. From sea ice phase relations (sea ice phase-diagram can be seen e.g. in [3]), it can be concluded, that for thermodynamic equilibrium the relative volume fraction of brine $\mathrm{n}^{\mathbf{L}}$ depends solely on the ice temperature θ and its bulk salinity S^{bulk}, see [5]. The brine volume fraction can be given according to [6] via the linearized relationship given in $(1)_2$. The weak formulations of the balance equations (mixture balance of momentum, mass balance salt, mass balance mixture, energy balance mixture) are prepared by a GALERKIN procedure and implemented into the Finite-Element-Code FEAP by Taylor [7], which solves the set of degrees of freedom $\mathcal{R} = \mathcal{R}(\mathbf{u_I}, S^{bulk}, \mathrm{p}^{\mathbf{L}\mathrm{R}}, \theta)$, with the solid ice deformation $\mathbf{u_I}$ and the liquid pressure $\mathrm{p}^{\mathbf{L}\mathrm{R}}$. With that, the temperature-salinity-equilibrium can be calculated for different fixed bulk salinities, which fits well with the results given in [5], see Fig. 9. Therein, the bulk salinities are given in parts per thousand [ppt], where the average ocean water salinity is at 35 ppt (35 g/kg). The bulk salinity for the biphasic pancake

* Corresponding author: e-mail andrea.thom@isd.uni-stuttgart.de, phone +49 711 685 69532, fax +49 711 685 63706

formation is composed as $S^{bulk} = \mathrm{n}^{\mathbf{I}}\, S^{ice} + \mathrm{n}^{\mathbf{L}}\, S^{br}$, where the salinity of the forming solid ice is nearly pure and so $S^{ice} \approx 0$. Hence, the bulk salinity depends on the varying volume fractions. The evolution and growth $\hat{\rho}^{alg}$ of sea ice algae c^{alg} in forming pancakes depend on different environmental conditions, so that in a phenomenological approach the maximum growth rate $\hat{\rho}^{alg}_{\max}$ is restricted by the following parameters:

$$\hat{\rho}^{alg} = \hat{\rho}^{alg}_{\max}\, f_{PAR}\, f_N\, f_S\, f_\theta\,, \tag{2}$$

see [4]. Therein, the limiting functions represent the dependence on light availability f_{PAR} (photosynthetic active radiation), nutrient availability f_N, salinity f_S and temperature f_θ. Nutrient limitation is modeled via MONOD kinetics, the salinity dependence (reduced growth rate of algae when exposed to salinities deviating from standard seawater values) with a power-log Gaussian fit and temperature dependence is based on a standard exponential formulation; all equations to be found in [4].

3 Academic example

For a numeric example a small block (0.01 x 0.01 x 0.01 m) of ocean water ($\mathrm{n}^{\mathbf{I}} \approx 0$, cf. Fig. 4) with an initial temperature of $\theta = -1.8°\mathrm{C}$ (freezing point ocean water) is cooled down at a small quadratic area on top (Fig. 3). It can be seen, that a

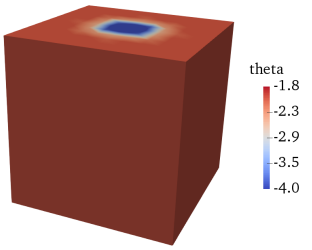

Fig. 3: Initial boundary value problem (IBVP) with $\Delta\,\theta = -4°$

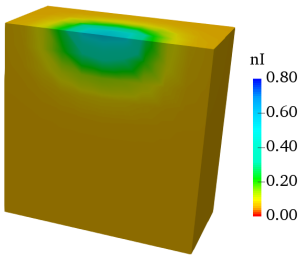

Fig. 4: Sectional view of volume fraction $\mathrm{n}^{\mathbf{I}}$ at start of simulation

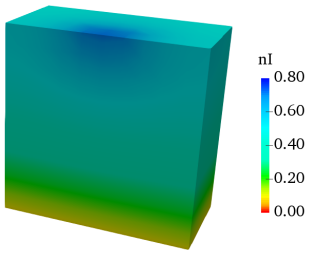

Fig. 5: Sectional view of volume fraction $\mathrm{n}^{\mathbf{I}}$ at steady state

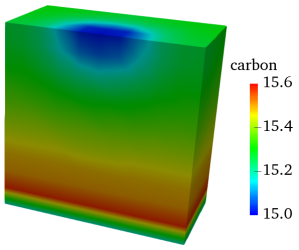

Fig. 6: Sectional view of assimilated carbon c^{alg} at steady state

steady state equilibrium is reached after a while with a maximum volume fraction of ice $\mathrm{n}^{\mathbf{I}} = 0.8$ at the top surface, see Fig. 5 and Fig. 7. The growth of sea ice algae can be monitored by the assimilated carbon of the phytoplankton. Starting with an initial value of $\mathrm{c}^{alg} = 15\,\mathrm{C\,mmol/m^3}$ and a maximum growth rate of $\hat{\rho}^{alg}_{\max} = 3.3 \cdot 10^5\,\mathrm{mmol/m^3\,s}$, the actual growth rate is controlled by the surrounding conditions of nutrient availability (here silicate), temperature and salinity. The growth rate and the limiting functions are plotted in Fig. 8. It shows, that the increasing salinity in the enclosed brine channels has the greatest

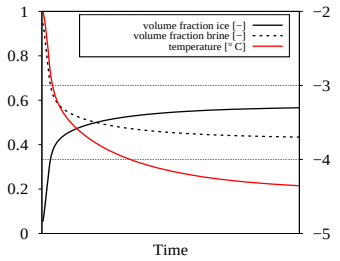

Fig. 7: Volume fractions $\mathrm{n}^{\mathbf{I}}$ and $\mathrm{n}^{\mathbf{L}}$ (left y-axis), temperature θ (right y-axis)

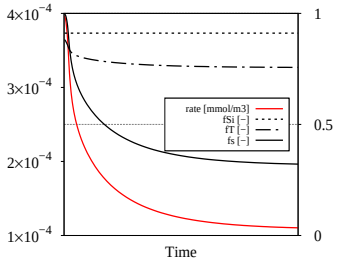

Fig. 8: Growth rate ice algae $\hat{\rho}^{alg}$ (left y-axis), rate limiting functions (right y-axis)

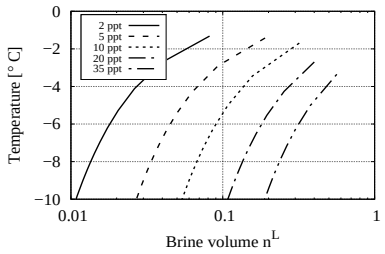

Fig. 9: Temperature-brine volume equilibrium for fixed bulk salinities S^{bulk}

impact, whereas nutrient availability is constant. The reduction of carbon assimilation due to increased salinity and lower temperature can also be observed in Fig. 6, where a cut in the middle of the cubic shows the carbon distribution at steady state. An accumulation of the ice algae at the bottom of the growing pancake can be monitored as it is also observed in nature.

Acknowledgements Open access funding enabled and organized by Projekt DEAL.

References

[1] T. Ricken, A. Sindern, J. Bluhm, M. Denecke, T. Gehrke, and T. C. Schmidt, Journal of Applied Mathematics and Mechanics **94**(7 – 8), 609 – 622 (2014).
[2] A. Thom and T. Ricken, PAMM – Proc. Appl. Math. Mech. **19**, e201900285 (2019).
[3] A. Assur, Composition of sea ice and its tensile strength (US Army Snow, Ice and Permafrost Research Establishment, 1960).
[4] M. Vancoppenolle and L. Tedesco, Sea Ice pp. 492–515 (2017).

[5] C. Petrich and H. Eicken, Sea ice pp. 1–41 (2017).
[6] C. M. Bitz and W. H. Lipscomb, Journal of Geophysical Research **C7**, 15699 – 15677 (1999).
[7] R. L. Taylor, Feap-a finite element analysis program, 2014.